Leucogranite genesis connected with low-pressure high-temperature metamorphism in the Sila basement (Calabria, Italy)

Autor(en): **Caggianelli, Alfredo / Moro, Aldo Del / Di Battista, Patrizia**

Objekttyp: **Article**

Zeitschrift: **Schweizerische mineralogische und petrographische Mitteilungen = Bulletin suisse de minéralogie et pétrographie**

Band (Jahr): **83 (2003)**

Heft 3

PDF erstellt am: **06.08.2024**

Persistenter Link: https://doi.org/10.5169/seals-63151

Schweizerische Mineralogische und Petrographische Mitteilungen 83, 301–316, 2003

Leucogranite genesis connected with low-pressure high-temperature metamorphism in the Sila basement (Calabria, Italy)

Alfredo Caggianelli[1], *Aldo Del Moro*[2], *Patrizia Di Battista*[1], *Giacomo Prosser*[3] and *Alessandro Rottura*[4]

Abstract

A Late-Hercynian intrusion of two-mica leucogranite from the Sila (Calabria, Italy) has been examined for petrographic, geochemical, and radiogenic isotope characteristics. The main objective was to analyse leucogranite genesis and its relation to partial melting of the Sila high-grade migmatitic paragneiss, which is affected by low-pressure metamorphism. The studied leucogranite is strongly peraluminous and is characterized by the presence of andalusite and sillimanite. It is very similar in major element composition to experimental melts produced by muscovite dehydration melting reaction from meta-sedimentary rocks. The leucogranite has high Rb and low Sr contents, whereas Zr and LREE concentrations are moderate to low. Variations in Sr, Rb, Zr, and LREE are inversely correlated to corresponding variations in migmatitic paragneiss. Maximum Zr and LREE contents in two leucogranite samples coherently indicate a saturation temperature of ca. 750 °C for both zircon and monazite. The estimate is in good agreement with peak temperatures of 740–770 °C obtained for high-grade rocks underlying the granite. These observations suggest a melt–restite connection between leucogranite and migmatitic paragneiss. Sr isotopic data are in agreement with this hypothesis whereas differences in the Nd isotopic composition between leucogranite and migmatitic paragneiss are attributed to disequilibrium retention of monazite in the residue. Mass-balance calculations, performed combining average major oxides analyses of leucogranite and migmatitic paragneiss, allow to reconstruct a composition similar to standard shale, except for the higher Na_2O/CaO ratio.

Keywords: Leucogranite, crustal anatexis, low-pressure metamorphism, monazite, Al-silicates, Calabria.

1. Introduction

According to recent experimental studies (Montel and Vielzeuf, 1997; Patiño Douce and Harris, 1998; Castro et al., 1999; Patiño Douce, 1999), peraluminous leucogranitic melts are typically produced by crustal anatexis. Geochemical and isotopic characteristics of worldwide leucogranites of different ages are generally in support of this hypothesis (e.g. Le Fort et al., 1987; France-Lanord et al., 1988; Inger and Harris, 1993; Harris et al., 1995; Williamson et al., 1996; Harrison et al., 1999; Visonà and Lombardo, 2002). However, there are also many examples in favour of an origin from highly fractionated melts of associated granodiorite–monzogranite magmas (e.g. Monier et al., 1984; Clarke et al., 1993; Tommasini et al., 1999).

Late-Hercynian two-mica Al-silicate leucogranites occur in the Calabria – Peloritani terrane (Bonardi et al., 2001). The main outcrops are located in the Sila and Aspromonte massifs (Calabria) and in the northeastern Peloritani Mountains (Sicily). Previous studies have produced controversial interpretations of the genesis of these leucogranites. For the Sila leucogranites Lorenzoni et al. (1979a,b) and D'Amico et al. (1982–83) favour an origin by partial melting of a metapelitic source. More recent interpretations (Messina et al., 1991a; Rottura et al., 1993; Ayuso et al., 1994), based on a geochemical and isotopic approach, suggest an origin by differentiation from the associate hybrid magmas of tonalitic to monzogranitic composition, which mainly contributed to the formation of the Sila batholith. In this paper, in view of recent experimental studies (e.g. Patiño Douce and Harris, 1998) and new ideas on the tectono-metamorphic evolution of the area (e.g. Grässner and Schenk, 2001), we reconsider the possibility that at least some Sila leucogranites may represent purely crustal melts.

The study is focused on the genesis of a leucogranite intrusion cropping out in Sila in the vi-

[1] Dipartimento Geomineralogico, Università di Bari, Italy. <caggianelli@geomin.uniba.it>
[2] Istituto di Geocronologia e Geochimica Isotopica, CNR Pisa, Italy.
[3] Dipartimento di Scienze Geologiche, Università della Basilicata, Potenza, Italy.
[4] Dipartimento di Scienze della Terra, Università di Bologna, Italy.

0036-7699/03/0083/301

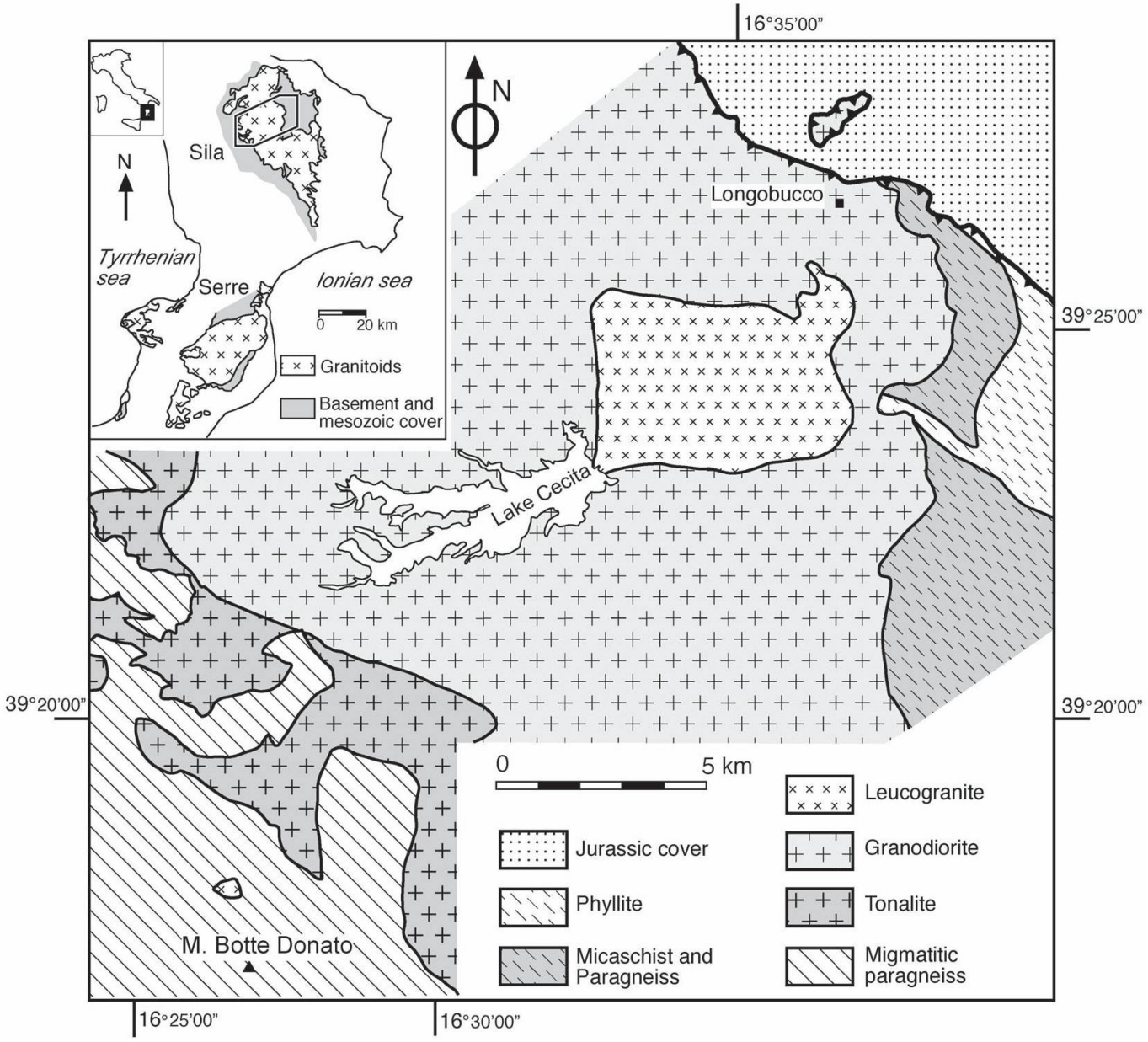

Fig. 1 Geological sketch map of the Sila Grande area. Study area framed in inset.

cinity of Lago Cecita (Fig. 1). This leucogranite shows compositional features quite similar to those of experimental melts obtained from micaceous source rocks (Patiño Douce and Harris, 1998). In addition high-grade metapelites in the Sila massif underwent partial melting during the late Hercynian low-pressure metamorphism (Grässner et al., 2000). This close association in space and time between low-pressure metamorphism and granitoid magmatism allows us to address two distinct perspectives: (i) the connection between magmatic heat advection and peak metamorphism; (ii) the connection between genesis of acidic melts and partial melting in high-grade rocks. The first topic has been treated by Caggianelli and Prosser (2002), the second topic is the subject of this paper.

2. Geological setting

The Calabria – Peloritani terrane is located between the Southern Apennines and the Sicilian Maghrebides (Bonardi et al., 2001). It mainly consists of crystalline nappes deriving from late-Hercynian continental crust and Alpine ophiolites. In the Sila massif (Fig. 1), a section of the continental crust from upper to intermediate depths is exposed (Grässner et al., 2000; Grässner and Schenk, 2001; Caggianelli and Prosser, 2001). The crustal section has been exhumed and tilted northeastwards during the Oligocene–Miocene, as documented by fission track dating on zircon and apatite (Thomson, 1994).

The upper level in the crustal section, as described by Borghi et al. (1992), consists of two tec-

tonic units juxtaposed prior to the intrusion of late-Hercynian granitoids. The upper tectonic unit is made up of phyllites with minor metavolcanic rocks, and is affected by a sharp contact aureole. The lower tectonic unit consists of micaschists and paragneisses that record peak metamorphism at T = 550–600 °C and P < 400 MPa. Here, contact metamorphic effects are difficult to discern from effects of regional low-pressure metamorphism. The age of metamorphism in both tectonic units is estimated at about 330 Ma by a Rb–Sr isochron on metavolcanic rocks (Acquafredda et al., 1992).

Late-Hercynian granitoid intrusions make up the central part of the cross-section; their cumulative thickness amounts to 7–9 km. Granitoids have calc-alkaline affinity and are represented by tonalite, granodiorite, monzogranite and leucogranite (Messina et al., 1991a), with a tendency for the more felsic types to prevail at shallow crustal levels. Tonalite usually shows a strong magmatic to subsolidus fabric, outlined by preferred orientation of plagioclase and biotite. A weaker fabric is characteristic of granodiorite and monzogranite, except for porphyritic types where magmatic alignment of feldspar megacrysts is well recognizable. Estimates of the ages of the Sila granitoid magmatism, determined by $^{40}Ar/^{39}Ar$ method on hornblende and muscovite, provided values spanning from 293 to 289 Ma (Ayuso et al., 1994). More recently, Grässner et al. (2000) dated Sila granitoids by the U–Pb method on zircon and monazite. They obtained ages on average 10–15 Ma older than $^{40}Ar/^{39}Ar$ estimates by Ayuso et al. (1994). In Sila, two-mica leucogranites represent later intrusions crosscutting the other granitoids (Lorenzoni et al., 1979a, b; Caggianelli and Prosser, 2001). They are medium to coarse grained and the preferred orientation of minerals is hardly recognizable. A muscovite age of 291 Ma was obtained by Ayuso et al. (1994) for a leucogranite from the zone studied here. Ayuso et al. (1994) concluded that all of the granitoids ultimately came from a mantle-derived parental magma that underwent contamination with crustal material. They also indicated that the entire chemical spectrum of the Sila granitoids could be produced by a combination of crystal fractionation and mixing between mantle- and crust-derived melts.

The lower level in the crustal section has a thickness of about 7 km and consists mainly of migmatitic paragneiss with minor metabasite and marble (Dubois, 1971; Lorenzoni and Zanettin Lorenzoni, 1983; Grässner and Schenk, 2001). Peak metamorphic conditions estimated for the migmatitic paragneiss are typical of low-pressure metamorphic belts and of the European late-Hercynian crust (Viezeuf and Pin, 1989). Grässner and Schenk (2001) estimated P = 400–600 MPa and T = 740–770 °C, while Grässner et al. (2000) dated the age of metamorphism at 300–304 Ma by U–Pb method on monazite. After peak metamorphism the lower part of the crustal section underwent minor decompression followed by isobaric cooling.

According to Caggianelli and Prosser (2002) peak metamorphism in migmatitic paragneiss can be related to the heat released by thick granitoid sheets intruded in the intermediate continental crust. Emplacement of granitoids took place during late orogenic extension which affected the European Hercynian belt after collision (Matte, 1991).

3. Petrography

The Sila two-mica leucogranites have equigranular medium to coarse grain size, rarely porphyritic for the presence of larger K-feldspar. Preferred orientation of feldspars is rarely discernible. The granitoids are leuco-monzogranitic in composition and devoid of magmatic mafic enclaves, in contrast to other Sila granitoids. Instead, they rarely contain millimetre-size clots of chlorite and white mica probably replacing former cordierite (Lorenzoni et al., 1979a).

K-feldspar can be interstitial or poikilitic enclosing all of the other phases. It commonly displays perthitic exsolutions and grid twinning. Plagioclase is euhedral to subhedral with compositions ranging from Ab_{98} to Ab_{92}. Quartz usually occurs in polycrystalline rounded aggregates, and the contacts between single grains are lobate. Biotite and muscovite content are generally low, down to 2% of the rock volume. The more felsic samples, displaying aplitic texture with micrographic intergrowth, contain elongate and randomly oriented biotite flakes (Fig. 2a), suggestive of rapid crystallization in an undercooled magma (e.g. Vernon, 1991). Muscovite shows textural features pointing to either primary or secondary crystallization. Possibly primary muscovite is represented by interstitial crystals and by euhedral flakes in textural equilibrium with biotite. Secondary muscovite grew at the expense of feldspar, Al-silicates and biotite. In the latter case, it typically shows opaque trails along cleavage planes.

Al-silicates are represented by andalusite and fibrolitic sillimanite. Andalusite occurs as partially resorbed crystals in muscovite (Fig. 2b), or as inclusion within feldspar (Messina et al., 1991b). Andalusite inclusions in K-feldspar are in some cases rimmed by muscovite and quartz (Fig. 2c).

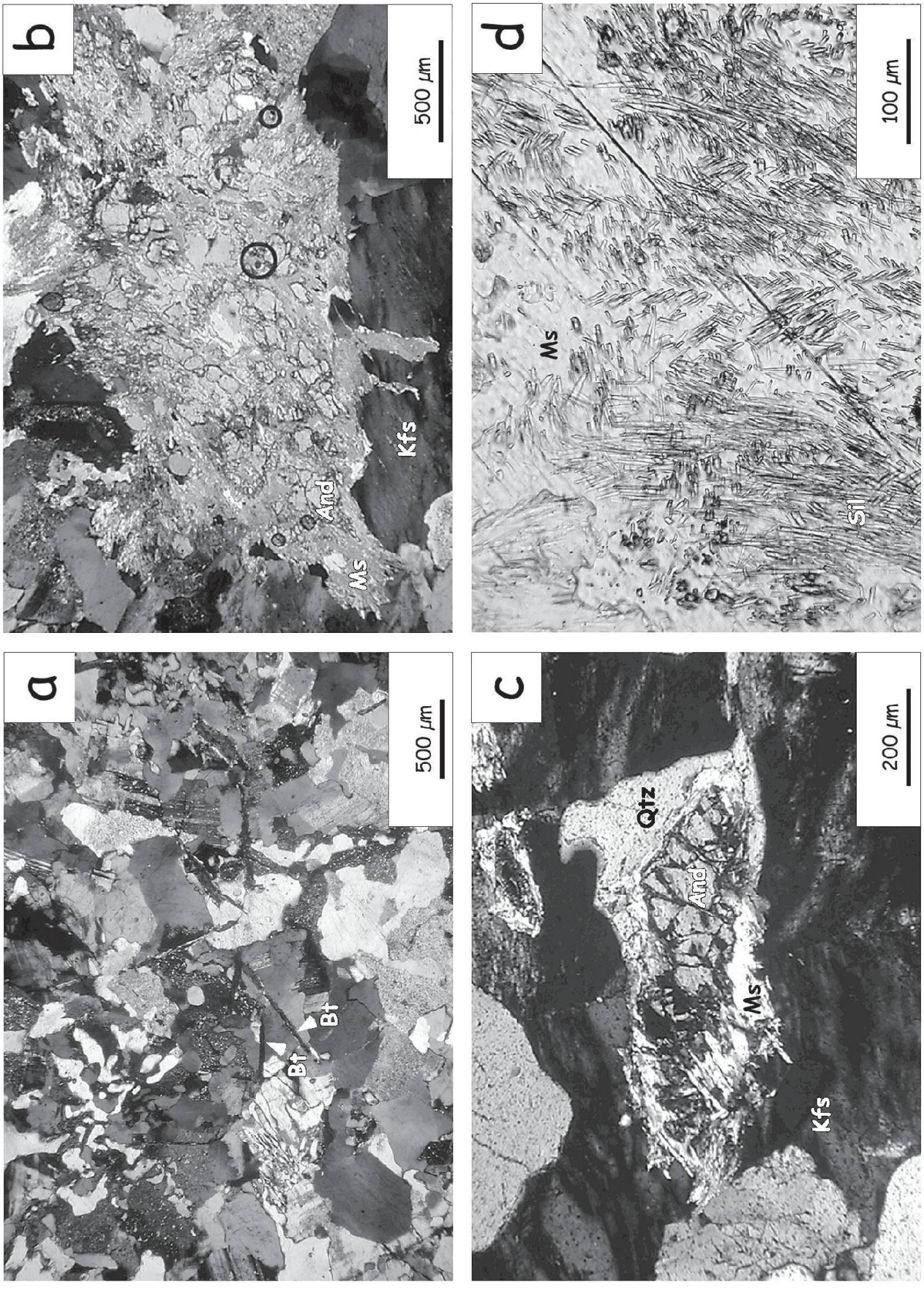

Fig. 2 Photomicrographs of two-mica leucogranites from the Sila. (a) Typical micrographic texture with elongate biotite (crossed polars). (b) Muscovite flake with inclusions of relic andalusite (crossed polars). (c) Reaction texture between andalusite and K-feldspar indicative of the subsolidus reaction: K-feldspar + andalusite + H_2O = muscovite + quartz (crossed polars). (d) Fibrolitic sillimanite showing a relic crenulation cleavage (plane-polarized light). Mineral symbols after Kretz (1983).

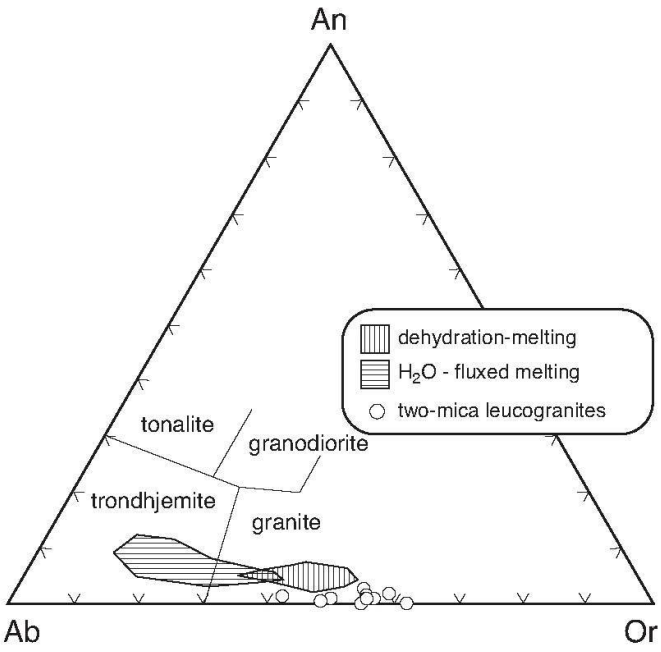

Fig. 3 Ternary feldspar normative classification diagram according to Barker (1979). The hatched areas indicate compositional ranges of experimentally generated melts (Patiño Douce and Harris, 1998).

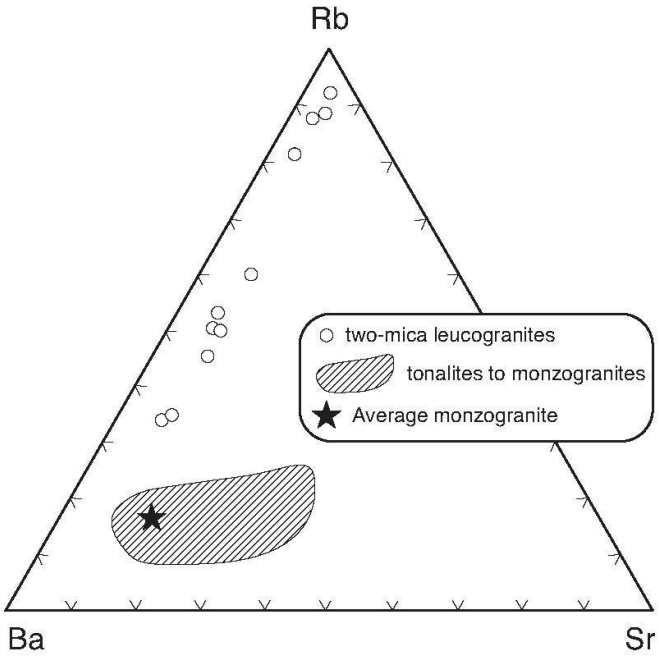

Fig. 4 Ba–Rb–Sr diagram for Sila leucogranites showing an extreme depletion in Sr and a variable Rb/Ba. The hatched area encloses data points representative of other Sila granitoids.

This texture indicates that the andalusite–K-feldspar interface became unstable during cooling owing to the well-known reaction:

$$\text{K-feldspar} + \text{andalusite} + H_2O = \text{muscovite} + \text{quartz}$$

Fibrolitic sillimanite occurs both as widespread and randomly oriented needles within quartz and feldspars, or in the shape of mats enclosed in muscovite. In the latter case fibrolite needles may outline a relic crenulation (Fig. 2d).

The occurrence of Al-silicates in Sila leucogranite was first reported by Lorenzoni et al. (1979a) who suggested a xenocrystic origin for these phases. More recently, Messina et al. (1991a, b) and Ayuso et al. (1994) proposed a magmatic origin for the Al-silicates. In general, andalusite in felsic peraluminous granite is considered as an accessory mineral of magmatic origin (e.g. Hills, 1938; Clarke et al., 1976; Crisci et al., 1979; Clarke, 1981; D'Amico et al., 1982/83). An analogous origin was suggested for fibrolite by Puglisi and Rottura (1973) in leucogranite from northeastern Peloritani mountains (Sicily). Pichavant et al. (1988) confirmed a magmatic origin of sillimanite in the Macusani ignimbrites. In the Sila two-mica leucogranite, a xenocrystic or restitic origin should be considered at least for the crenulated mats of sillimanite. Ascent and emplacement of leucogranite magma mostly took place through thick granitoid bodies. Therefore, it can be excluded that sillimanite formation is related to assimilation of wall rocks. A magmatic origin seems unlikely for the randomly oriented fibrolite needles, as well. In fact, according to experimental results, sillimanite needles enclosed in the main phases can be produced during muscovite dehydration melting reactions (Patiño Douce and Harris, 1998). In conclusion, we infer a restitic origin for the fibrolite, probably related to partial melting reactions taking place in the underlying high-grade metapelites.

The original presence of cordierite is suggested by the occurrence of pinite pseudomorphs enclosed in muscovite. Apatite is the most common accessory phase and is followed in abundance by zircon, monazite and xenotime. Among the accessory phases, apatite displays a larger grain size. Zircon and monazite typically are found as inclusions in biotite but also in feldspar and quartz, and are contained in very low amounts in the more felsic types.

4. Geochemical and isotopic features and their implications for leucogranite petrogenesis

4.1. Major and trace element geochemistry

The samples of the studied two-mica leucogranites have silica contents ranging from 70.57 to 76.75 wt% (Table 1). The sum TiO_2+FeO+MgO ranges from 2.58 to 0.62 wt%. Low values of this sum are typical of leucogranites and of experimental melts generated by muscovite dehydra-

Table 1 Major and trace element composition of Sila two-mica leucogranite. Average compositions of associated monzogranite (AMG; n = 6) and experimental glass (AEG; n = 5; Patiño Douce and Harris, 1998) obtained by partial melting of a metapelitic source are shown for comparison. Analyses of major oxides (by ICP AES) and trace elements (by ICP MS) for the Sila samples were performed at Actlabs®.

	BOC27	BOC28	BOC38	BOC39	BOC41	BOC42	BOC44	BOC45	BOC46	BOC47	BOC73	AMG	AEG
wt%													
SiO_2	72.89	73.13	72.18	72.92	73.33	75.20	76.75	75.61	70.98	74.04	70.57	72.18	74.66
TiO_2	0.06	0.05	0.18	0.12	0.13	0.06	0.03	0.04	0.21	0.05	0.11	0.23	0.14
Al_2O_3	14.70	14.55	13.76	13.31	13.65	12.82	13.38	13.71	14.43	13.94	15.46	14.84	15.63
Fe_2O_3	1.14	0.73	2.09	1.91	1.67	1.07	0.57	0.84	1.86	0.98	2.12	2.24	1.03
MnO	0.02	0.01	0.04	0.04	0.03	0.02	0.01	0.03	0.01	0.03	0.03	0.04	0.04
MgO	0.12	0.12	0.52	0.31	0.35	0.14	0.08	0.08	0.37	0.16	0.29	0.51	0.27
CaO	0.45	0.24	0.36	0.20	0.23	0.12	0.13	0.26	0.42	0.29	0.54	0.77	0.73
Na_2O	3.39	2.63	2.69	3.29	3.10	3.13	3.30	3.93	2.94	3.07	3.31	3.35	3.75
K_2O	4.84	6.10	5.58	4.91	5.51	5.39	4.40	4.11	5.52	5.49	5.85	3.92	3.87
P_2O_5	0.27	0.18	0.12	0.10	0.08	0.08	0.07	0.08	0.25	0.10	0.15	0.14	–
LOI	0.84	0.81	1.16	1.73	0.64	0.65	0.88	0.76	1.55	0.79	0.81	1.18	–
tot	98.72	98.55	98.67	98.84	98.72	98.67	99.59	99.46	98.54	98.94	99.24	99.41	100.12
ppm													
Cs	5.0	2.1	3.6	2.7	3.9	2.8	4.1	4.2	6.0	3.4	0.9	3.2	
Ba	13	45	359	185	169	218	32	18	251	135	272	628	
Rb	304	248	210	218	219	214	322	243	301	251	167	158	
Sr	12	12	43	29	25	40	13	13	48	33	38	127	
Rb/Sr	25.3	20.7	4.9	7.5	8.8	5.4	24.8	18.7	6.3	7.6	4.4	1.2	
La	2.5	3.0	23.1	16.3	19.3	9.71	5.8	5.7	24.6	7.2	21.1	34.4	
Ce	5.0	5.5	49.3	35.4	39.7	19.9	12.0	12.1	45.8	15.6	43.1	63.6	
Pr	0.6	0.8	5.3	4.2	4.5	2.2	1.8	1.5	6.0	1.8	4.9	7.7	
Nd	2.3	3.2	20.6	15.4	17.9	8.9	7.1	6.0	23.4	6.9	19.2	29.2	
Sm	0.9	1.2	5.0	3.8	5.0	2.4	2.3	2.4	5.8	2.1	5.1	5.7	
Eu	0.07	0.13	0.38	0.23	0.26	0.27	0.09	0.10	0.45	0.24	0.3	0.84	
Gd	1.2	1.0	4.6	3.5	5.2	2.4	2.7	3.2	4.6	2.4	4.3	4.8	
Tb	0.3	0.2	0.8	0.7	1.0	0.5	0.6	0.8	0.6	0.5	0.6	0.6	
Dy	1.4	1.0	4.6	4.0	6.2	2.8	3.5	5.3	2.4	2.9	3.2	3.2	
Ho	0.2	0.1	0.8	0.7	1.2	0.6	0.7	1.1	0.3	0.5	0.5	0.5	
Er	0.6	0.4	2.5	2.2	3.5	1.7	2.2	3.5	0.7	1.7	1.2	1.4	
Tm	0.1	0.1	0.4	0.4	0.6	0.3	0.4	0.6	0.1	0.3	0.2	0.2	
Yb	0.5	0.5	2.4	2.2	3.3	1.8	2.5	3.8	0.4	1.6	0.8	1.2	
Lu	0.05	0.08	0.35	0.31	0.50	0.26	0.37	0.63	0.03	0.28	0.06	0.15	
ΣREE	15.7	17.2	120.1	89.3	108.2	53.7	42.1	46.7	115.2	44.0	104.6	153.5	
Y	8	5	27	23	38	19	24	36	10	18	16	17	
Th	1.3	2.7	15.2	10.8	15.1	6.1	4.6	6.3	16.0	5.3	6.5	14.4	
U	5.3	3.0	2.5	2.3	2.8	2.2	2.8	4.5	4.4	2.9	1.8	2.2	
Zr	21	33	96	59	48	45	31	54	94	43	49	124	
Hf	1.0	1.9	3.3	2.2	2.0	1.8	1.7	3.1	3.1	1.8	2.2	3.7	
Ta	2.2	0.6	2.1	2.0	2.1	1.2	2.2	1.5	1.6	0.7	1.5	0.9	
Tl	1.6	1.5	1.1	1.3	1.3	1.1	2.2	1.3	1.7	1.3	1.0	1.1	
Sc	3	2	5	5	4	2	5	2	2	2	4	5	
Co	3	4	5	4	5	4	7	2	4	4	2	5	
Ga	23	18	18	18	16	14	22	16	21	15	24	19	
M[1]	1.13	1.20	1.17	1.25	1.32	1.25	1.26	1.22	1.29	1.23	1.30		
D[2]	0.94	0.97	0.95	1.02	1.08	1.02	1.05	1.00	1.04	1.01	1.03		
T_{Zr}[3]	676	646	678	754	711	700	695	711	750	693	699		
T_{REE}[4]	688	622	636	765	729	751	694	675	763	685	755		
T_{REE}[5]	666	603	616	740	705	726	672	654	738	663	730		

[1] M parameter in Watson and Harrison (1983) equation.
[2] D parameter in Montel (1983) equation.
[3] Zircon saturation temperature in °C calculated with Watson and Harrison (1983) equation.
[4] Monazite saturation temperature in °C calculated with Montel (1993) equation assuming 4 wt% water in melt.
[5] Monazite saturation temperature in °C calculated with Montel (1993) equation assuming 8 wt% water in melt.

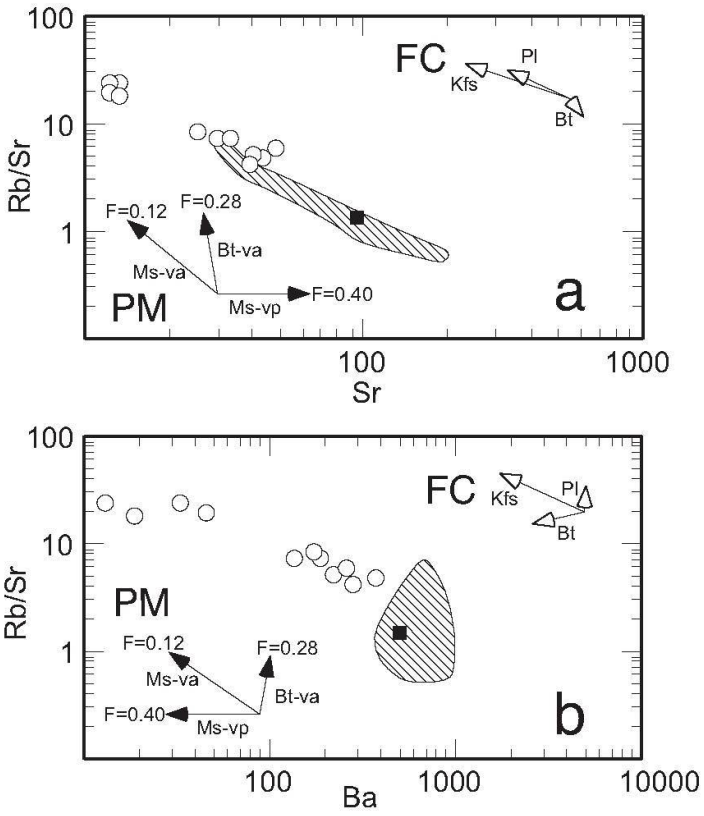

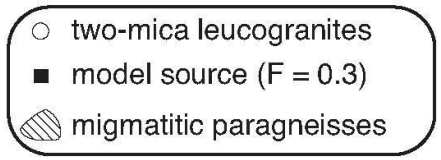

Fig. 5 (a) Rb/Sr–Sr and (b) Rb/Sr–Ba Log-Log diagrams. Vectors indicate model trends according to calculations by Inger and Harris (1993) for the case of fractional crystallization (FC) and partial melting (PM). The hatched area indicates compositions of migmatitic paragneiss. The solid square represents the composition of the model source rock obtained imposing 30% partial melting (F) (see discussion on the possible source rocks). va—vapor absent; vp—vapor present. Mineral symbols after Kretz (1983).

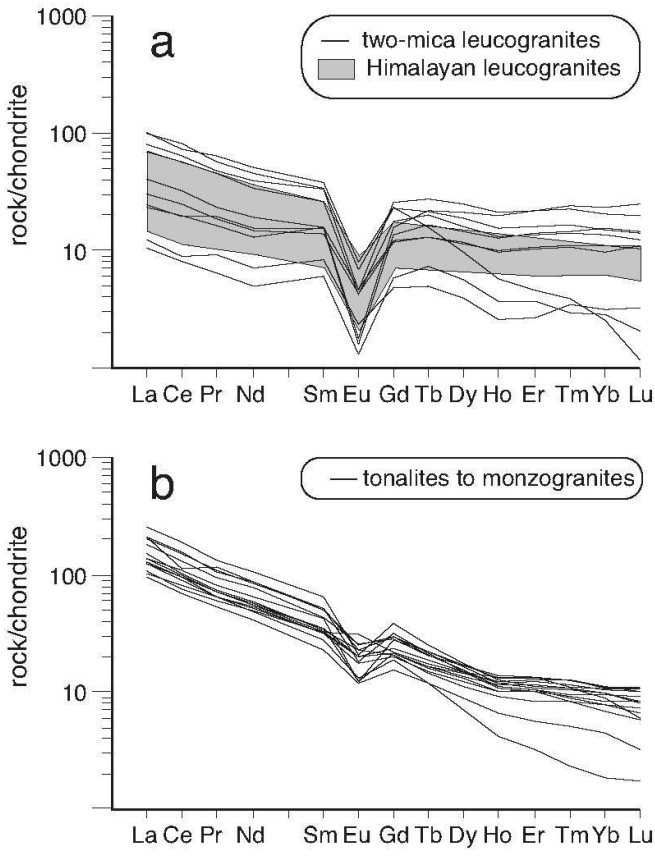

Fig. 6 (a) REE patterns for the Sila leucogranites. The grey area encompasses patterns of selected Himalayan leucogranites (Dietrich and Gansser, 1981; France-Lanord and Le Fort, 1988). (b) REE patterns for the other Sila granitoids. Normalizing values after McDonough and Sun (1995).

tion reaction from a metapelite source (Patiño Douce, 1999). The rocks are strongly peraluminous with values of A/CNK (Al_2O_3/[CaO +Na_2O+K_2O] molecular ratio) varying from 1.15 to 1.28. K_2O and Na_2O are negatively correlated, and the K_2O/Na_2O ratio ranges from 1.0 to 2.3.

In the CIPW normative feldspar diagram (Fig. 3), our two-mica leucogranite samples plot close to the Ab–Or join, as a consequence of the very low An contents. In addition, they plot close to the field of experimental melts obtained by muscovite dehydration melting (Patiño Douce and Harris, 1999), from which they differ in their lower An and slightly higher Or contents.

To investigate compositional variability of the studied leucogranite intrusion, we focused mostly on Ba, Rb and Sr contents, considering that the behaviour of these trace elements is determined by the rock-forming minerals and is not influenced by accessory phases (McCarthy and Hasty, 1976).

The two-mica leucogranite samples show high contents of Rb and low contents of Ba, Sr, and Zr. These characteristics are distinctive with respect to the associated monzogranites having comparable silica content (Table 1). In particular, Sr concentration in leucogranite ranges from 48 to 12 ppm, and is significantly lower than in associated monzogranites, with an average value of 127 ppm (Table 1). The Rb–Ba–Sr diagram (Fig. 4) shows that Sr is low and that the Rb/Ba ratio is characterized by a wide variation from 0.6 to 23, being

decidedly higher than in the associated monzogranites (0.25).

Data points in the Rb/Sr–Sr and Rb/Sr–Ba diagrams (Fig. 5) define linear trends, characterized by an increase of Rb/Sr and a concomitant decrease of Ba and Sr, very similar to those found in Himalayan leucogranites. Inger and Harris (1993) examined two alternative hypotheses to explain these trends: (i) partial melting by vapor-absent breakdown of muscovite or, (ii) K-feldspar crystal fractionation (Fig. 5). Textural and mechanical reasons led Inger and Harris (1993) to exclude the hypothesis that K-feldspar crystal fractionation occurs in the leucogranite system. Instead, covariation of Rb/Sr vs. Ba is related to the proportion of K-feldspar in the residue during the melting process. Melts with high Rb/Sr and low Ba and Sr would be related to a K-feldspar-rich residue, whereas melts with lower Rb/Sr and higher Ba and Sr would be related to a K-feldspar-poor residue.

Growing proportions of K-feldspar in the residue are related to the progressive incongruent melting of muscovite in response to low a_{H2O}. By contrast, high a_{H2O} would consume large amounts of feldspar in the melting reaction. In the Sila massif, both Ba-poor leucogranites and the pres-

Table 2 Selected EDS analyses of monazite (ΣO = 4).

	Migmatitic paragneiss BOC 65					Leucogranite BOC 38			
wt%									
P_2O_5	29.05	27.62	27.76	28.79	27.89	28.06	28.71	28.22	27.31
SiO_2	0.24	0.18	0.05	0.03	0.43	1.13	0.78	0.72	0.87
TiO_2	<0.01	0.29	0.14	<0.01	<0.01	<0.01	0.07	<0.01	<0.01
ThO_2	3.87	2.64	1.98	4.56	3.72	8.02	6.60	5.61	3.79
UO_2	0.93	0.69	0.75	0.98	0.55	0.30	0.97	0.04	0.04
Al_2O_3	0.09	0.06	<0.01	0.25	<0.01	<0.01	<0.01	<0.01	0.01
Y_2O_3	1.07	0.68	1.96	3.14	1.90	1.89	2.72	1.13	0.93
La_2O_3	15.63	14.66	16.01	14.06	15.47	10.71	11.82	12.46	13.50
Ce_2O_3	28.67	27.54	27.41	26.71	27.98	23.77	25.86	26.96	29.73
Pr_2O_3	2.46	4.03	3.27	2.33	3.34	3.23	2.90	3.75	3.57
Nd_2O_3	11.81	12.68	12.03	11.06	11.40	12.69	12.37	13.19	13.86
Sm_2O_3	1.65	2.97	2.96	2.45	2.53	3.22	2.72	2.24	2.79
Gd_2O_3	1.02	2.17	2.41	1.74	1.59	1.47	0.90	0.93	0.81
FeO	0.92	0.32	0.29	0.14	<0.01	0.44	0.09	0.49	0.42
MnO	0.01	0.17	0.66	0.51	0.35	0.46	<0.01	<0.01	0.04
MgO	<0.01	0.18	<0.01	0.24	0.05	0.20	<0.01	<0.01	<0.01
CaO	0.68	0.63	0.33	0.87	0.51	2.00	1.09	1.33	0.14
PbO	0.28	0.28	0.06	0.57	0.30	0.44	0.57	0.52	0.22
total	98.39	97.80	98.05	98.42	98.01	98.04	98.18	97.59	98.02
formula(ΣO=4)									
P	0.98	0.96	0.96	0.97	0.96	0.95	0.97	0.96	0.95
Si	0.01	0.01	<0.01	<0.01	0.02	0.05	0.03	0.03	0.04
Ti	<0.01	0.01	<0.01	<0.01	<0.01	<0.01	<0.01	<0.01	<0.01
Th	0.04	0.02	0.02	0.04	0.03	0.07	0.06	0.05	0.04
U	0.01	0.01	0.01	0.01	<0.01	<0.01	0.01	<0.01	<0.01
Al	<0.01	<0.01	<0.01	0.01	<0.01	<0.01	<0.01	<0.01	<0.01
Y	0.02	0.01	0.04	0.07	0.04	0.04	0.06	0.02	0.02
La	0.23	0.22	0.24	0.21	0.23	0.16	0.17	0.19	0.20
Ce	0.42	0.41	0.41	0.39	0.42	0.35	0.38	0.40	0.45
Pr	0.04	0.06	0.05	0.03	0.05	0.05	0.04	0.06	0.05
Nd	0.17	0.19	0.18	0.16	0.17	0.18	0.18	0.19	0.20
Sm	0.02	0.04	0.04	0.03	0.04	0.04	0.04	0.03	0.04
Gd	0.01	0.03	0.03	0.02	0.02	0.02	0.01	0.01	0.01
Fe	0.03	0.01	0.01	<0.01	<0.01	0.01	<0.01	0.02	0.01
Mn	<0.01	0.01	0.02	0.02	0.01	0.02	<0.01	<0.01	<0.01
Mg	<0.01	0.01	<0.01	0.01	<0.01	0.01	<0.01	<0.01	<0.01
Ca	0.03	0.03	0.01	0.04	0.02	0.09	0.05	0.06	0.01
Pb	<0.01	<0.01	<0.01	0.01	<0.01	<0.01	0.01	0.01	<0.01
Σcat	2.01	2.03	2.03	2.03	2.02	2.04	2.00	2.02	2.02

Analyses were done by a Cambridge S360 SEM equipped with a Link AN 10000 ED detector hosted in Dipartimento Geomineralogico, University of Bari. Operating conditions were 15 kV accelerating potential, 1 nA probe current. Standards used: Minerals and pure components manufactured by Micro-Analysis Consultants Ltd.

ence of K-feldspar in the residual assemblage of migmatitic paragneiss (Grässner and Schenk, 2001) are consistent with partial melting under moderate to low a_{H2O}.

Two-mica leucogranite samples show a wide range of ΣREE (from 15 to 120 ppm) with mostly parallel and weakely fractionated patterns, and 9 out of 11 samples having $[La/Yb]_N$ lower than 7 (Fig. 6a). Only sample BOC 46 shows a highly fractionated pattern ($[La/Yb]_N$ = 40) resulting from the dominant contribution of monazite. Typically, the leucogranites display a prominent Eu negative anomaly with average Eu/Eu* of 0.23. The observed profiles, despite their wide range in REE contents, are comparable in shape with selected patterns of Himalayan leucogranites (Fig. 6a). Compared to associated Sila granitoids (Fig. 6b) the leucogranite data show significant differences with higher contents in ΣREE (from 101 to 264 ppm), steeper REE patterns ($[La/Yb]_N$ = 20.4 on the average) and less pronounced Eu anomalies (Eu/Eu* = 0.66 on the average).

4.2. Zircon and monazite saturation in leucogranite melt

Most leucogranites are characterized by moderate to low contents in Zr and LREE. In the Sila leucogranite, Zr and LREE are almost exclusively carried by zircon and monazite. Therefore, leucogranite melt saturation in zircon and monazite can be estimated following models by Watson (1979) and Montel (1993), respectively.

The Zr concentration required to stabilize zircon depends on temperature and on the composition parameter M = (2Ca + Na + K)/(Si×Al) (Watson and Harrison, 1983). The typical value of M for a granitic composition is ca. 1.3. For the analysed Sila two-mica leucogranite samples, M has an average value of 1.24 ± 0.06. The equation provided by Watson and Harrison (1983) is:

$$\ln (Zr_{zircon} / Zr_{melt}) = -3.8 - 0.85 \times (M-1) + 12900/T\ [K]$$

where Zr_{zircon} is set to 476,000 ppm.

According to Montel (1993) solubility of REE in a granitic melt equilibrating with monazite depends on temperature, H_2O content and a composition parameter D = (Na + K + Li + 2Ca)/(Al×(Al+Si)). For the Sila two-mica leucogranite samples the average value of D is 1.01 ± 0.04. It should be pointed out that Li content was not measured for the studied samples, as its influence on D is generally negligible. The equation provided by Montel to calculate REE solubility is:

$$\ln(REEtot/X_{REEPO4}) = 9.50 + 2.34 \times D + 0.3879 \times (H_2O)^{1/2} - 13318/T\ [K]$$

where REEtot = $\Sigma_i REE_i$ (ppm)/at. wt. and is calculated for La to Gd excluding Eu; H_2O is in wt% and X_{REEPO4} is the mole fraction of REE phosphate in monazite. According to Montel (1993), the typical value of X_{REEPO4} in monazites from peraluminous granites is 0.83. Nine monazite EDS analyses in leucogranite sample BOC 38 (Table 2) provided values of X_{REEPO4} spanning from 0.80 to 0.97 and an average of 0.90, used here for calculations. For the H_2O content, we assumed

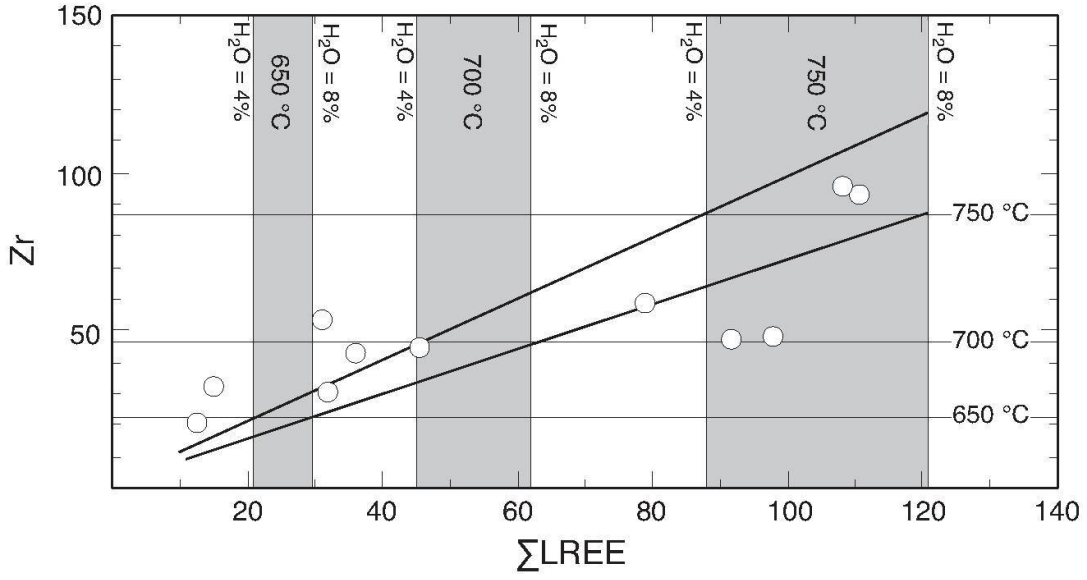

Fig. 7 Zr–ΣLREE diagram with saturation temperatures for zircon and monazite according to models by Watson (1996) and Montel (1993), respectively. The upper oblique line indicates simultaneous saturation in zircon and monazite when water content in the melt is 4 wt%. The lower line is for a water content of 8 wt%.

values ranging from 4 to 8 wt%, compatible with estimates of water concentrations in model haplogranite partial melts formed under fluid-absent conditions (Clemens and Watkins, 2001).

Zr and LREE show positive covariation in the Sila two-mica leucogranite (Fig. 7). Saturation temperatures for zircon range from 646 to 754 °C. Saturation temperatures for monazite range from 622 to 765 °C and from 603 to 740, for water contents of 4 and 8 wt%, respectively.

Of the eleven leucogranite samples only five could be simultaneously saturated in zircon and monazite for water contents in the magma between 4 and 8 wt%, as shown in Fig. 7. Two of them indicate equilibrium temperatures close to 750 °C, a realistic value for the initial thermal condition of the magma. This temperature is consistent with estimates of the peak metamorphism (T = 740–770 °C at P = 400–600 MPa) for the Sila migmatitic paragneisses (Grässner and Schenk, 2001) which are regionally considered as the residue left after removal of peraluminous granitic melts (Schenk, 1990; Caggianelli et al., 1991). As outlined before, the Sila leucogranite has characteristics consistent with an origin by muscovite dehydration melting of metapelites. At the low-pressure conditions recorded in the migmatitic paragneisses from Sila, a temperature of 750 °C may be appropriate to trigger muscovite dehydration melting, owing to the positive slope in a P–T diagram of the reaction:

$$Ms + Qtz \pm Pl = Als + Kfs + melt.$$

Lower temperatures deduced for the other samples can be explained with (a) leucogranite magma evolution by crystal fractionation at decreasing temperatures, and/or with (b) undersaturation of the leucogranite melt related to partial retention of monazite and zircon in the restite.

Mechanism (a) implies crystallization of zircon and monazite in a temperature range of >110 °C. Considering realistic H_2O concentrations (4 to 8 wt%), leucogranite melt should be water saturated at the estimated shallow level of emplacement (about 250 MPa according to Caggianelli et al., 1999). Experimental investigations on melting/crystallization of natural granites in H_2O-saturated conditions carried out by Winkler and Schultes (1982) indicate a crystallization temperature interval of 50–60 °C, considerably lower than 110 °C. Moreover, the saturation temperatures of zircon and monazite may be affected by variations in the M and D parameters in the equations given above. However, the variations in major oxide composition observed in the analyzed

Table 3 Sr isotopic data for select samples of Sila two-mica leucogranite and two samples of migmatitic paragneiss. $^{87}Sr/^{86}Sr$ initial ratios were calculated at 290 Ma, based on age data by Ayuso et al. (1994).

	Rb	Sr	$^{87}Rb/^{86}Sr$	$^{87}Sr/^{86}Sr \pm 2\sigma$	$(^{87}Sr/^{86}Sr)_{290} \pm 2\sigma$
two-mica leucogranites					
BOC38	210	43	14.22	0.770586 ± 9	0.7119 ± 6
BOC44	322	13	73.43	0.959749 ± 36	0.6567 ± 30
BOC45	243	13	55.29	0.935576 ± 51	0.7074 ± 23
BOC46	301	48	18.29	0.788752 ± 18	0.7133 ± 8
BOC47	251	33	22.21	0.803946 ± 32	0.7123 ± 2
BOC73	167	38	12.78	0.761462 ± 18	0.7087 ± 5
migmatitic paragneisses					
BOC65	110	83	3.84	0.728151 ± 20	0.7123 ± 2
BOC89	28	101	0.803	0.720772 ± 12	0.7175 ± 1

Table 4 Nd isotopic data for select samples of Sila two-mica leucogranite and two samples of migmatitic paragneiss.

	Sm	Nd	$^{147}Sm/^{144}Nd$	$^{143}Nd/^{144}Nd \pm 2\sigma$	$(^{143}Nd/^{144}Nd)_{290}$	$(\varepsilon_{Nd})_{290} \pm 2\sigma$
two-mica leucogranites						
BOC38	5.04	20.6	0.148	0.512155 ± 11	0.511874	–7.6 ± 0.4
BOC44	2.3	7.08	0.196	0.512293 ± 19	0.511923	–6.7 ± 0.6
BOC45	2.35	5.99	0.237	0.512345 ± 16	0.511895	–7.2 ± 0.7
BOC46	5.78	23.4	0.149	0.512122 ± 9	0.511839	–8.3 ± 0.2
BOC47	2.1	6.85	0.185	0.512233 ± 9	0.511881	–7.5 ± 0.5
migmatitic paragneisses						
BOC65	14	71.1	0.119	0.511969 ± 9	0.511743	–10.2 ± 0.4
BOC89	7.15	34	0.127	0.512070 ± 7	0.511829	–8.5 ± 0.4

samples are modest and thus of insignificant influence. In addition, evolution by crystal fractionation would require a simultaneous saturation in zircon and monazite during evolution, a condition not satisfied by six out of eleven samples. Finally, some of the estimated saturation temperatures for monazite are too low for melt to be present.

According to mechanism (b) the low concentration in Zr and LREE in some leucogranites may be linked to processes taking place in the source region. High concentrations of Zr and LREE detected in some migmatitic paragneiss indicate significant retention of zircon and monazite in the residue (Table 2). Average Zr and LREE concentrations amount to 263 and 254 ppm, with maximum values of 383 and 460 ppm, respectively. Residual biotite containing monazite or zircon has not been observed in leucogranite. Most leucogranite melts could thus be undersaturated in zircon and/or monazite leading to underestimation of temperatures by accessory phase thermometry.

4.3. Sr–Nd isotopes

Six leucogranite samples were analysed for Rb–Sr isotopes. Data points do not fit a reliable line on a Rb–Sr isochron diagram. A better solution is gained if sample BOC 44, characterized by the highest value of $^{87}Rb/^{86}Sr$, is excluded from calculation. In this case an age of 284 ± 14 Ma is obtained with a corresponding $^{87}Sr/^{86}Sr$ initial ratio of 0.713 ± 0.006 (Fig. 8). The quite large errors indicate that Sr isotope mobilization took place to variable extents in leucogranite. Nonetheless, the calculated line satisfactorily fits data points representative of the migmatitic paragneiss, considered as potential restites after removal of leucogranite melt. This result, considered together with field relations and the available $^{40}Ar/^{39}Ar$ date of 291 Ma (Ayuso et al., 1994), might suggest that the studied leucogranite has an age younger than the other Sila granitoids (300–304 Ma, according to Grässner et al., 2000). For this reason we decided to calculate intial ratios at 290 Ma (Table 3).

$^{87}Sr/^{86}Sr$ initial ratios range from 0.6567 to 0.7133 (Table 3). The unrealistically low values and wide range confirm Sr isotope mobilization, and in particular ^{87}Sr loss. As stressed by Williamson et al. (1996), this is typical of rocks with high $^{87}Rb/^{86}Sr$ (from 12.78 to 73.43 in the analysed samples). Three out of six samples (BOC38, BOC46 and BOC47) display clear crustal features (from 0.7119 to 0.7133) and may be compared with potential restites. Two Sila migmatitic paragneisses have $^{87}Sr/^{86}Sr$ initial ratios at 290 Ma of 0.7123 and 0.7175 (Table 3), while five migmatitic paragneisses from the Serre massif (southern Calabria) show values ranging from 0.7115 to 0.7147 (see Caggianelli et al., 1991). Nonetheless, we consider these data with extreme care, owing to the errors affecting estimates of $^{87}Sr/^{86}Sr$ initial ratios.

ε_{Nd} values, calculated at 290 Ma, span from –6.7 to –8.3 in leucogranite and from –8.5 to –10.2 in the Sila migmatitic paragneiss (Table 4). Therefore, leucogranite retains a less pronounced Nd

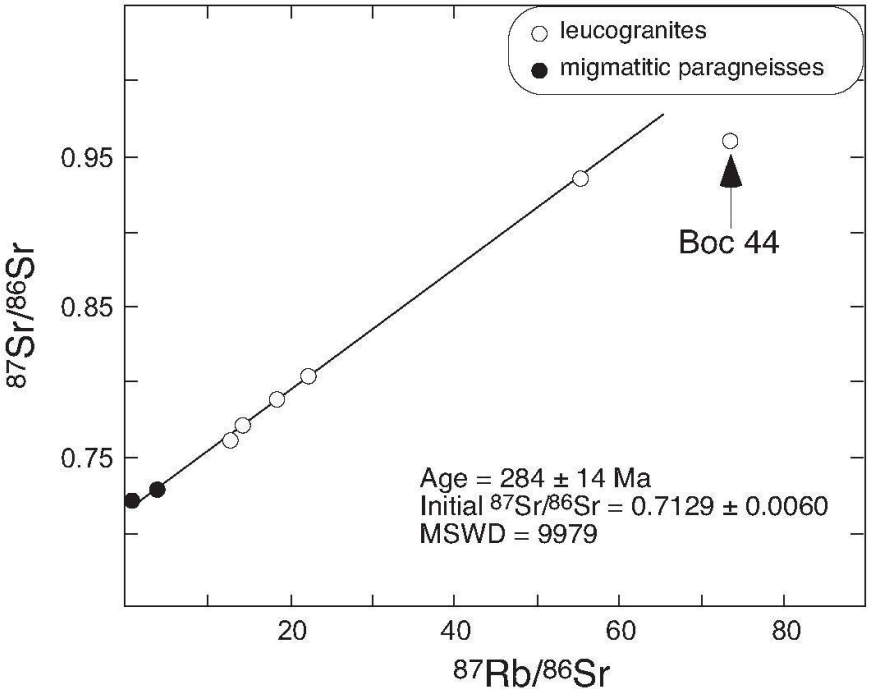

Fig. 8 $^{87}Sr/^{86}Sr$ versus $^{87}Rb/^{86}Sr$ plot. The isochron was calculated for leucogranites, excluding sample Boc 44. Data points representative of the migmatitic paragneisses lie close to the isochron line.

Table 5 Results of mass balance calculations to reconstruct the source rock composition in a partial melting model. All compositions were recalculated on an anhydrous basis. Average compositions of migmatitic paragneiss (column 1) and two-mica leucogranite (2) were combined imposing weight fractions of melt (F) of 0.2, 0.3 and 0.4 (columns 5–7). Compositions of Calabrian pelite calculated by Schenk (1990) (8) and PAAS (Taylor and McLennan, 1985) (9) are included for comparison.

	Leucogranites (n = 11)		Migmatitic paragneisses (n = 12)		F = 0.2	F = 0.3	F = 0.4	PAAS	Calculated Calabrian pelite
	Av.	σ	Av.	σ					
wt%									
SiO_2	75.07	1.66	59.22	9.81	63.29	63.98	65.56	64.17	63.4
TiO_2	0.10	0.06	1.30	0.38	1.06	0.94	0.82	1.02	0.68
Al_2O_3	14.29	0.77	22.11	6.48	20.55	19.76	18.98	19.31	19.1
FeO	1.24	0.53	8.96	2.51	7.42	6.64	5.87	6.64	6.4
MnO	0.03	0.01	0.13	0.05	0.11	0.10	0.09	0.11	–
MgO	0.24	0.15	2.97	0.86	2.42	2.15	1.88	2.25	2.8
CaO	0.30	0.14	0.88	0.68	0.76	0.71	0.65	1.33	1.8
Na_2O	3.23	0.35	1.47	0.88	1.82	2.00	2.17	1.23	2.5
K_2O	5.37	0.64	2.87	1.05	3.37	3.62	3.87	3.78	3.3
P_2O_5	0.14	0.07	0.10	0.03	0.11	0.11	0.12	0.16	
ppm									
Cs	3.5	1.4	2.6	1.2	2.8	2.9	3.0	15.0	
Ba	154	117	579	226	494	452	409	650	
Rb	245	47	112	45	139	152	165	160	
Sr	28	14	105	60	90	82	74	200	
La	12.6	8.4	62.4	21.1	52.4	47.5	42.5	38.0	
Ce	25.8	17.0	121.0	39.1	102.0	92.4	82.9	80.0	
Pr	3.1	1.9	13.4	4.2	11.3	10.3	9.3	8.9	
Nd	11.9	7.6	51.7	16.0	43.7	39.8	35.8	32.0	
Sm	3.3	1.7	10.0	2.9	8.7	8.0	7.3	5.6	
Eu	0.23	0.12	1.65	0.50	1.37	1.22	1.08	1.1	
Gd	3.2	1.4	8.7	2.4	7.6	7.1	6.5	4.7	
Tb	0.6	0.2	1.2	0.4	1.1	1.0	1.0	0.77	
Dy	3.4	1.6	7.1	2.2	6.4	6.0	5.6	4.4	
Ho	0.6	0.3	1.4	0.5	1.3	1.2	1.1	1.0	
Er	1.8	1.1	4.4	1.5	3.9	3.6	3.2	2.9	
Tm	0.3	0.2	0.6	0.2	0.6	0.5	0.5	0.4	
Yb	1.8	1.2	4.0	1.3	3.5	3.3	3.1	2.8	
Lu	0.26	0.20	0.60	0.21	0.53	0.50	0.46	0.43	
ΣREE	69	39	288	89	244	222	200	183	
Y	20	10	42	15	38	35	33	27	
Th	8.2	5.2	21.6	6.5	18.9	17.6	16.2	14.6	
U	3.1	1.1	3.2	1.1	3.2	3.2	3.2	3.1	
Zr	52	24	276	58	231	209	186	210	
Hf	2.2	0.7	7.7	1.5	6.6	6.1	5.5	5.0	
Nb	8.2	3.5	17.9	7.0	16.0	15.0	14.0	19.0	
Ta	1.6	0.6	1.4	0.7	1.4	1.5	1.5	–	
Tl	1.2	0.3	0.8	0.5	0.9	0.9	1.0	–	
Sc	3	1	23	8	19	17	15	10	
Co	4	1	24	7	20	18	16	–	
Ga	19	3	30	11	27	27	26	–	

isotopic crustal signature compared to migmatitic paragneiss. This mismatch may be related to monazite behaviour during partial melting. More or less effective retention of monazite in the residue, owing to biotite armouring (Nabelek and Glascock, 1995) or slow dissolution in melt (Watt and Harley, 1993), could be responsible for the low concentrations of LREE in leucogranite magma, as outlined in the previous section. According to Nabelek and Glascock (1995), disequilibrium melting involving monazite could potentially affect the Nd isotopic ratio of melts relative to coexisting residue. Similar conclusions were reached by Chavagnac et al. (2001) who attributed lack of

're-setting' of the Sm–Nd systematics during migmatization to retentivity of accessory minerals, such as apatite and monazite during anatexis. With the minor contribution of monazite, the Sm/Nd and $^{143}Nd/^{144}Nd$ ratios of the melt could be significantly influenced also by major phases participating in the melting reaction. Figure 9 shows that samples with lower contents in LREE and thus in monazite are characterized by higher values of Sm/Nd and $^{143}Nd/^{144}Nd$, and less negative ε_{Nd} values. This covariation supports the hypothesis that monazite behaviour during melting determined the $^{143}Nd/^{144}Nd$ mismatch between melt and residue.

5. Possible source rocks

Assuming that metasediments underlying granitoids represent restites after removal of leucogranite magma, mass balance calculations were performed to reconstruct the original source rock. This was done by adding increasing amounts of the average leucogranite composition to the average restite (Table 5). The major problem with this approach is related to the variability in composition of the restite, as represented by migmatitic paragneiss. It is assumed that this variability depends in large amount on the efficiency of restite–melt separation. This assumption seems justified by the good fit of data points to linear trends in major oxides scatter diagrams, a feature coherent with the melt–restite unmixing model. To obtain a composition close to the average post-Archean Australian shale (PAAS by Taylor and Mclennan, 1985) 0.2 to 0.4 weight proportions of leucogranite are needed. The optimum value as estimated by least squares calculations is 0.3 ($\Sigma R^2 = 1.095$). Considering major oxides the model source rock appears different from PAAS for the lower CaO and higher Na_2O contents. Regarding trace elements, Cs, Ba and Sr are depleted, whereas Sc and Y are enriched. In Fig. 10, the REE pattern of the model source rock is compared with leucogranite, restite and PAAS patterns. In comparison to PAAS the model pattern is characterized by a more pronounced Eu anomaly and by higher contents in HREE. The increasingly negative Eu anomaly in going from the model source to the leucogranitic melt precludes a massive participation of plagioclase in the melting reaction. The wide difference between restite and leucogranite confirms that a major role in the distribution of REE was played by accessory phases such as monazite and zircon which preferentially partitioned into the residue.

Similar studies carried out by Schenk (1990) and Caggianelli et al. (1991) in the Serre massif (Fig. 1) also indicate a restite – granite connection. For example, Schenk (1990) obtained a composition very close to average pelite (Table 5), by combining 60% of migmatitic paragneiss and

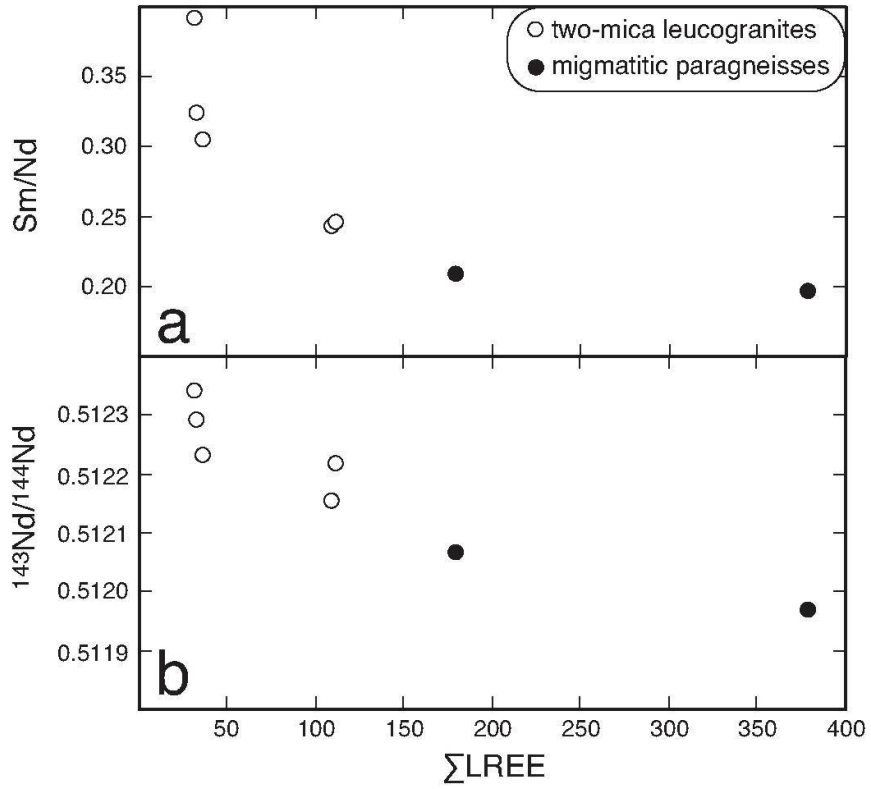

Fig. 9 (a) Sm/Nd and (b) $^{143}Nd/^{144}Nd$ are negatively correlated with LREE in leucogranites and migmatitic paragneisses. This feature is attributed to preferential retention of monazite in the residue.

40% of peraluminous granite. The higher melt fraction compared to this study can be related to more widespread biotite dehydration melting reactions in the Serre massif.

6. Conclusions

In general, extreme compositions, such as those of the Sila two-mica leucogranite, are compatible both with crystal fractionation from a hybrid granodiorite – monzogranite melt, or partial melting of crustal material. Discriminating between these alternative hypotheses is a difficult task because the two processes are theoretically able to produce similar compositions. However, careful analysis by Ayuso et al. (1994) revealed that AFC modelling could not reproduce the Rb-rich and Co-poor compositions of the Sila leucomonzogranites. For this reason they admitted that a significant sedimentary component was present in the source region of peraluminous monzogranite and that the mantle component was restricted. The data collected in this study, in light of the new experimental evidence (Patiño Douce and Harris, 1998) and the new tectono-metamorphic evolution proposed for the Sila massif (Grässner and Schenk, 2001), appear consistent with an origin by partial melting of crustal material. In this context, some important points emerge from this study:

– Leucogranite major element composition is close to experimental melts obtained from a metapelite source through muscovite dehydration melting.

– Zircon and monazite saturation models indicate a temperature of ca. 750 °C. This is in agreement with the estimated peak metamorphic conditions in the underlying migmatitic paragneisses (Grässner and Schenk, 2001). Low concentrations of Zr and LREE observed in most leucogranites are thought to be related to zircon and monazite retention in the residue. This is supposed by petrographic observations and by the high content in Zr and LREE in the migmatitic paragneisses, considered as the restite counterpart.

– High $^{87}Rb/^{86}Sr$ ratio in leucogranites is a source of error in the Sr isotopic analysis. However, excluding the sample with the highest $^{87}Rb/^{86}Sr$, a reasonable isochron (284 ± 14 Ma) can be obtained. Interestingly, data points representative of the migmatitic paragneisses lie close to this isochron, indicating that they could really represent the restite after extraction of the leucogranite melt. On the other hand, the general assumption of the same ε_{Nd} in melt and restite could be inadequate in the studied case. In fact, different values of ε_{Nd} data in leucogranites with respect to restites could be related to disequilibrium distribution of monazite during the melting process.

– Combining the average compositions of leucogranites and migmatitic paragneisses, by mass balance calculations, a possible source rock can be reconstructed. With respect to a standard shale (PAAS), it was obtained a composition with a

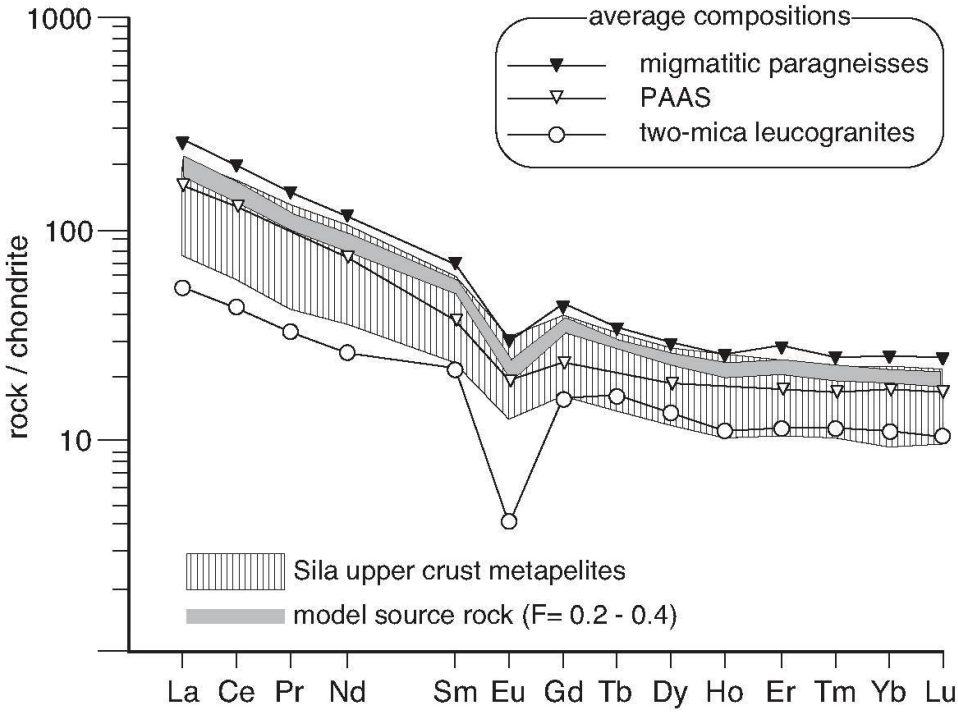

Fig. 10 Model REE pattern of the source rock (grey) reconstructed combining, by mass balance, average compositions of migmatitic paragneiss and leucogranite, and imposing a degree of partial melting (F) varying from 0.2 to 0.4. Patterns of PAAS (Taylor and McLennan, 1985) and Sila upper crustal metapelite are shown for comparison.

higher Na_2O/CaO ratio, a more pronounced negative Eu anomaly and a higher content in HREE. The degree of partial melting, estimated by least squares method, is 0.3.

– The close spatial association of the leucogranite to the main Sila tonalite–granodiorite to monzogranite bodies, is a last important point. This association is found also in other segments of the Hercynian belt, such as those exposed in the basement of the Italian southern Alps (D'Amico and Rottura, 1982/83; Rottura et al., 1998). Even there, leucogranites represent pure anatectic melts associated to hybrid tonalites and granodiorites. We propose that the genesis of the leucogranite magma is related to low-pressure metamorphism and crustal anatexis triggered by the intrusion of the main hybrid magmas in the intermediate to upper crust.

Acknowledgements

The paper benefited from constructive reviews by Volker Schenk and an anonymous referee and from helpful suggestions by editor Martin Engi. Pasquale Acquafredda's assistance in EDS analyses of monazite is gratefully acknowledged. Financial support came from funds of Bari, Basilicata, and Bologna Universities.

References

Acquafredda, P., Barbieri, M., Lorenzoni, S., Trudu, C. and Zanettin Lorenzoni, E. (1992): Metamorphism of the Mandatoriccio Unit in the context of the Hercynian and pre-Hercynian evolution of the Calabrian-Peloritan Arc (Southern Italy). *Rend. Fis. Acc. Lincei* **3**, 151–161.

Ayuso, R.A., Messina, A., De Vivo, B., Russo, S., Woodruff, L.G., Sutter, J.F. and Belkin, H.E. (1994): Geochemistry and argon thermochronology of the Variscan Sila Batholith, southern Italy: source rocks and magma evolution. *Contrib. Mineral. Petrol.* **117**, 87–109.

Barker, F. (1979): Trondhjemite: definition, environment and hypotheses of origin. In: Barker, F. (ed): Trondhjemites, Dacites and related rocks. *Developments in Petrology* **6**, Elsevier, Amsterdam, 1–12.

Bonardi, G., Cavazza, W., Perrone, V. and Rossi, S. (2001): Calabria-Peloritani terrane and northern Ionian Sea. In: Martini, I.P and Vai, G.B. (eds.): Anatomy of a Mountain Chain: the Apennines and Adjacent Mediterranean Basins. Kluwer, Dordrecht, 287–306.

Borghi, A., Colonna, V. and Compagnoni, R. (1992): Structural and metamorphic evolution of the Bocchigliero and the Mandatoriccio complexes in the Sila Nappe (Calabrian-Peloritan Arc, southern Italy). In: Carmignani, L. and Sassi, F.P. (eds): Contributions to the geology of Italy with Special Regard to the Palaeozoic Basements. *IGCP Newsletter*, Siena **276**, 321–334.

Caggianelli, A., Del Moro, A., Paglionico, A., Piccarreta, G., Pinarelli, L. and Rottura, A. (1991): Lower crustal granite genesis connected with chemical fractionation in the continental crust of Calabria (southern Italy). *Eur. J. Mineral.* **3**, 159–180.

Caggianelli, A., Prosser, G. and Bentivenga, M. (1999): A profile across the Hercynian continental crust in the Sila massif: inferences on crustal differentiation processes. *Plinius* **22**, 81–83.

Caggianelli, A. and Prosser, G. (2001): An exposed cross-section of Late-Hercynian upper and intermediate continental crust in the Sila nappe (Calabria, S. Italy). *Per. Mineral.* **70**, 277–301.

Caggianelli, A. and Prosser, G. (2002): Thermal perturbation of the continental crust after intraplating of thick granitoid sheets: a comparison with the crustal sections in Calabria (Italy). *Geol. Mag.* **139**, 699–706.

Castro, A., Patiño Douce, A.E., Corretge, L.G., de la Rosa, J.D., El-Biad, M. and El-Hmidi, H. (1999): Origin of peraluminous granites and granodiorites, Iberian massif, Spain: An experimental test of granite petrogenesis. *Contrib. Mineral. Petrol.* **135**, 255–276.

Chavagnac, V., Kramers, J.D., Nägler, T.F. and Holzer, L. (2001): The behaviour of Nd and Pb isotopes during 2.0 Ga migmatization in paragneisses of the Central Zone of the Limpopo Belt (South Africa and Botswana). *Precambr. Res.* **112**, 51–86.

Clarke, D.B. (1981): The mineralogy of peraluminous granites: a review. *Can. Mineral.* **19**, 3–17.

Clarke, D.B., McKenzie, C.B., Mueke, G.K. and Richardson, S.W. (1976): Magmatic andalusite from the South Mountain batholith, Nova Scotia. *Contrib. Mineral. Petrol.* **56**, 279–287.

Clarke, D.B., MacDonald, M.A., Reynolds, P.H. and Longstaffe, F.J. (1993): Leucogranites from the eastern part of the South Mountain Batholith, Nova Scotia. *J. Petrol.* **34**, 653–679.

Clemens, J.D. and Watkins, J.M. (2001): The fluid regime of high-temperature metamorphism during granitoid magma genesis. *Contrib. Mineral. Petrol.* **140**, 600–606.

Crisci, G., Maccarrone, E. and Rottura, A. (1979): Cittanova peraluminous granites (Calabria, Southern Italy). *Mineral. Petrog. Acta* **23**, 279–302.

D'Amico C. and Rottura, A. (1982–83): Occurrence of late-Hercynian peraluminous granites in the Southern Alps. *Rend. Soc. Ital. Mineral. Petrol.* **38**, 27–33.

D'Amico, C., Rottura, A., Bargossi, G.M. and Nannetti, M.C. (1982–83): Magmatic genesis of andalusite in peraluminous granites. Examples from Eisgarn-type granites in Mondanubikum. *Rend. Soc. Ital. Mineral. Petrol.* **38**, 15–25.

Dietrich, V. and Gansser, A. (1981): The leucogranites of the Bhutan Himalaya (crustal anatexis versus mantle melting). *Schweiz. Mineral. Petrog. Mitt.* **61**, 177–202.

Dubois, R. (1971): Définition d'un socle antéhercynien en Calabre. *C. R. Acad. Sci. Paris* **272**, 2052–2055.

France-Lanord, C. and Le Fort, P. (1988): Crustal melting and granite genesis during the Himalayan collision orogenesis. *Trans. Royal Soc. Edinburgh, Earth Sci.* **79**, 183–195.

France-Lanord, C., Sheppard, S.M.F. and Le Fort, P. (1988): Hydrogen and oxygen isotope variations in High Himalaya peraluminous Manaslu leucogranite: evidence for heterogeneous sedimentary source. *Geochim. Cosmochim. Acta* **52**, 513–526.

Grässner, T., Schenk, V., Bröcker, M. and Mezger, K. (2000): Geochronological constraints on the timing of granitoid magmatism, metamorphism and post-metamorphic cooling in the Hercynian crustal cross-section of Calabria. *J. Metamorphic Geol.* **18**, 409–421.

Grässner, T. and Schenk, V. (2001): An exposed Hercynian deep crustal section in the Sila Massif of Northern Calabria: mineral chemistry, petrology and a P–T path of granulite-facies metapelitic migmatites and metabasites. *J. Petrol.* **42**, 931–961.

Harris, N., Ayres, M. and Massey, J. (1995): Geochemistry of granitic melts produced during the incongruent

melting of muscovite: implications for the extraction of Himalayan leucogranite magmas. *J. Geophys Res.* **100 B8**, 15767–15777.
Harrison, T.M., Grove, M., Mc Keegan, K.D., Coath, C.D., Lovera, O.M. and Lefort, P. (1999): Origin and episodic emplacement of the Manaslu intrusive complex, Central Himalaya. *J. Petrol.* **40**, 3–19.
Hills, E.S. (1938): Andalusite and sillimanite in uncontaminated igneous rocks. *Geol. Mag.* **75**, 296–304.
Inger, S. and Harris, N. (1993): Geochemical constraints on leucogranite magmatism in the Langtang Valley, Nepal Himalaya. *J. Petrol.* **34**, 345–368.
Kretz, R. (1983): Symbols of rock-forming minerals. *Am. Mineral.* **68**, 277–279.
Le Fort, P., Cuney, M., Deniel, C., France-Lanord, C., Sheppard, S.M.F, Upreti, B.N. and Vidal, P. (1987): Crustal generation of the Himalayan leucogranites. *Tectonophysics* **134**, 39–57.
Lorenzoni, S., Messina, A., Russo, S., Stagno, F. and Zanettin Lorenzoni, E. (1979a): The two-mica Al_2SiO_5 granites of the Sila (Calabria). *N. Jb. Mineral. (Mh.)* **9**, 421–436.
Lorenzoni, S., Messina, A., Russo, S., Stagno, F. and Zanettin Lorenzoni, E. (1979b): Le magmatiti dell'unità di Longobucco (Sila – Calabria). *Boll. Soc. Geol. Ital.* **97**, 727–738.
Lorenzoni, S. and Zanettin Lorenzoni, E. (1983): Note illustrative della carta geologica della Sila alla scala 1:200000. *Mem. Sci. Geol. Padova* **36**, 317–342.
Matte, P. (1991): Accretionary history and crustal evolution of the Variscan belt in Western Europe. *Tectonophysics* **196**, 309–337.
McCarthy, T.S. and Hasty, R.A. (1976): Trace element distribution patterns and their relationship to the crystallization of granitic melts. *Geochim. Cosmochim. Acta* **40**, 1351–1358.
Mc Donough, W.F. and Sun, S. (1995): The composition of the Earth. *Chem. Geol.* **120**, 223–253.
Messina, A., Barbieri, M., Compagnoni, R., De Vivo, B., Perrone, V., Russo, S. and Scott, B.A. (1991a): Geological and petrochemical study of the Sila nappe granitoids. *Boll. Soc. Geol. Ital.* **110**, 165–206.
Messina, A., Russo, S., Perrone, V. and Giacobbe, A. (1991b). Calc-alkaline late-Variscan two mica-cordierite-Al-silicate-bearing intrusions of the Sila batholith (northern sector of the Calabrian-Peloritan arc, Italy). *Boll. Soc. Geol. Ital.* **110**, 365–389.
Monier, G., Mergoil-Daniel, J. and Labernardière, H. (1984): Génération successives de muscovites et feldspaths potassiques dans les leucogranites du massif de Millevaches (Massif Central français). *Bull. Minéralogique* **107**, 55–68.
Montel, J.M. (1993): A model for monazite/melt equilibrium and application to the generation of granitic melts. *Chem. Geol.* **110**, 127–146.
Montel, J.M. and Vielzeuf, D. (1997): Partial melting of metagreywackes, part II. Compositions of minerals and melts. *Contrib. Mineral. Petrol.* **128**, 176–196.
Nabelek, P.I. and Glascock, M.D. (1995): REE-depleted leucogranites, Black Hills, South Dakota: a consequence of disequilibrium melting of monazite-bearing schists. *J. Petrol.* **36**, 1055–1071.
Patiño Douce, A.E. and Harris, N. (1998): Experimental constraints on Himalayan anatexis. *J. Petrol.* **39**, 689–710.
Patiño Douce, A.E. (1999): What do experiments tell us about the relative contributions of crust and mantle to the origin of granitic magmas? In: Castro, A., Fernandez, C. and Vigneresse, J.L (eds): Understanding granites: integrating new and classical techniques. *Geol. Soc. London, Spec. Publ.* **168**, 55–75.
Pichavant, M., Kontak, D.J., Herrera, J.V. and Clark, A.H. (1988): The Miocene-Pliocene Macusani volcanics, SE Peru I. Mineralogy and magmatic evolution of a two-mica aluminosilicate-bearing ignimbrite suite. *Contrib. Mineral. Petrol.* **100**, 300–324.
Puglisi, G. and Rottura, A. (1973): Le leucogranodioriti muscovitiche della zona di Capo Rasocolmo (Messina). *Per. Mineral.* **42**, 207–256.
Rottura, A., Bargossi, G.M., Caggianelli, A., Del Moro, A., Visona', D. and Tranne, C.A. (1998): Origin and significance of the Permian high-K calc-alkaline magmatism in the central-eastern Southern Alps. *Lithos* **45**, 329–348.
Rottura, A., Caggianelli, A., Campana, R. and Del Moro, A. (1993): Petrogenesis of Hercynian peraluminous granites from the Calabrian Arc, Italy. *Eur. J. Mineral.* **5**, 737–754.
Schenk, V. (1990): The exposed crustal section of southern Calabria, Italy: structure and evolution of a segment of Hercynian crust. In: Salisbury, M.H. and Fountain, D.M. (eds.): Exposed cross-sections of the continental crust. Kluwer, Dordrecht, 21–42
Taylor, S.R. and McLennan, S.M. (1985): The continental crust: its composition and evolution. Oxford, Blackwell, 312 pp.
Thomson, S.N. (1994): Fission track analysis of the crystalline basement rocks of the Calabrian Arc, southern Italy: evidence of Oligo-Miocene late-orogenic extension and erosion. *Tectonophysics* **238**, 331–352.
Tommasini, S., Poli, G. and Ghezzo, C. (1999): Trace element inferences on the evolution and genesis of the Monte Pulchiana leucogranites, northern Sardinia, Italy. *Per. Mineral.* **68**, 53–67.
Vernon, R.H. (1991): Interpretation of microstructures of microgranitoid enclaves. In: Didier, J. and Barbarin, B. (eds): Enclaves and granite petrology, Elsevier, Amsterdam, 277–291.
Vielzeuf, D. and Pin, C. (1989): Geodynamic implications of granulite rocks in the Hercynian belt. In: Daly, J.S., Cliff, R.A. and Yardley, B.W.D. (eds.): Evolution of metamorphic belts. *Geol. Soc. Spec. Publ.* **43**, 343–348.
Visonà, D. and Lombardo, B. (2002): Two-mica and tourmaline leucogranites from the Everest-Makalu region (Nepal–Tibet). Himalayan leucogranite genesis by isobaric heating? *Lithos* **62**, 125–150.
Watson, B. (1979): Zircon saturation in felsic liquids: experimental data and applicaations to trace element geochemistry. *Contrib. Mineral. Petrol.* **70**, 407–419.
Watson, B. (1996): Dissolution, growth and survival of zircons during crustal fusion: kinetic principles, geological models and implications for isotopic inheritance. *Trans. Royal Soc. Edinburgh* **87**, 43–56.
Watson, E.B. and Harrison, T.M. (1983): Zircon saturation revisited: temperature and composition effects in a variety of crustal magma types. *Earth Planet. Sci. Lett.* **64**, 295–304.
Watt, G. and Harley, S.L. (1993): Accessory phase controls on the geochemistry of crustal melts and restites produced during water-undersaturated partial melting. *Contrib. Mineral. Petrol.* **114**, 550–566.
Williamson, B.J., Shaw, A., Downes, H. and Thirlwall, M.F. (1996): Geochemical constraints on the genesis of Hercynian two-mica leucogranites from the Massif Central, France. *Chem. Geol.* **127**, 25–42.
Winkler, H.G.F. and Schultes, H. (1982): On the problem of alkali feldspar phenocrysts in granitic rocks. *N. Jb. Mineral. (Mh.)* **12**, 558–564.

Received 29 November 2002
Accepted in revised form 22 December 2003
Editorial handling: M. Engi